Electronic Supplementary Material (ESI) for Chemical Science.
This journal is © The Royal Society of Chemistry 2020

Polymorph Exploration of Bismuth Stannate Using First-Principles Phonon Mode Mapping — Supplementary Information

Warda Rahim,[*,†,‡] Jonathan M. Skelton,[¶] Christopher N. Savory,[†,‡] Ivana R. Evans,[§] John S. O. Evans,[§] Aron Walsh,[‖,⊥] and David O. Scanlon[†,‡,#]

†*Department of Chemistry, University College London, 20 Gordon Street, London WC1H 0AJ, United Kingdom*

‡*Thomas Young Centre, University College London, Gower Street, London WC1E 6BT, United Kingdom*

¶*Department of Chemistry, University of Manchester, Oxford Road, Manchester M13 9PL, United Kingdom*

§*Department of Chemistry, University Science Site, Durham University, South Road, Durham DH1 3LE, United Kingdom*

‖*Department of Materials, Imperial College London, Exhibition Road, London SW7 2AZ,United Kingdom*

⊥*Department of Materials Science and Engineering, Yonsei University, Seoul 03722, Korea*

#*Diamond Light Source Ltd., Diamond House, Harwell Science and Innovation Campus, Didcot, Oxfordshire OX11 0DE, United Kingdom*

E-mail: d.scanlon@ucl.ac.uk

Computational Methodology

Pseudopotential plane-wave density functional theory (DFT),[1] as implemented in the Vienna *Ab initio* Simulation Package (VASP) code,[2–5] was used in this study to evaluate the structural and dynamical properties of $Bi_2Sn_2O_7$.

The projector augmented wave (PAW) method[6,7] was used to model the nuclei and core electrons, with the Bi $6s^26p^35d^{10}$, Sn $5s^25p^24d^{10}$ and O $2s^22p^4$ electrons included in the valence region. Electron exchange and correlation was modelled using the revised version of the Perdew-Burke-Ernzerhof generalized gradient approximation (GGA) functional for solids, PBEsol.[8] Convergence of the total energy per atom was checked with respect to both the plane-wave kinetic-energy cutoff and the k-point sampling using a convergence criterion of $\Delta E \approx 1$ meV per atom, resulting in a cutoff of 650 eV, increased by 1.3 $\times$ to avoid Pulay stress,[9] and Γ-centred Monkhorst-Pack k-meshes[10] with 3×3×3, 2×2×3, 2×2×1 and 3×3×2 subdivisions for the γ, β, α_{old} and α_{new} structures, respectively. The atomic positions, cell shapes and volumes were relaxed until the forces acting on the ions converged to $< 10^{-4}$ eV/Å. The equilibrium geometries were found to be in excellent agreement with experiment,[11–13] with < 1 % deviation on the optimised lattice parameters.

For lattice-dynamics calculations we used the supercell finite-displacement method[14,15] to calculate the second order interatomic force constants (IFCs), using the `Phonopy` package[16,17] and a finite-displacement step of 10^{-2} Å. The IFCs were used to compute the athermal (0 K) harmonic phonon dispersion curves and inspect them for imaginary modes. The presence of imaginary modes indicates that the structure is a local energy maximum on the structural potential-energy surface (PES) and thus that spontaneous atomic displacements, without any energetic barriers, convert the structure to a more stable phase. Imaginary modes at the Γ wavevector (the Brillouin zone centre) indicate distortions that are commensurate with the primitive unit cell, i.e. that the lower-energy structure does not require a change in the cell volume. Imaginary modes at other high-symmetry **q**-points - i.e. zone boundary phase transitions - indicate distortions that are commensurate with supercell expansions of

the primitive cell and for which the lower-energy structure therefore requires an expansion of the cell volume.

The eigenvectors of the imaginary harmonic modes lead to lower-energy structures *via* continuous collective atomic displacements. "Following" the imaginary modes, i.e. mapping the potential energy as a function of distortion amplitude along the eigenvector, can be used to characterise the PES and locate the energy minimum along the mode. The Cartesian displacement X_j of the jth atom along a phonon mode with amplitude Q is obtained from the real part of the eigenvector according to Eq. (1).

$$X_j = \frac{Q}{\sqrt{N_a m_j}} \mathrm{Re}[\exp(i\phi)\mathbf{e}_j \exp(\mathbf{q}.\mathbf{r}_{jl})] \tag{1}$$

Q is the normal-mode coordinate (distortion amplitude). $\mathbf{r}_{jl}$ and m_j are respectively the position and mass of the jth atom in the lth unit cell, and N_a is the total number of atoms in the supercell. $\mathbf{e}_j$ is the jth component of the phonon-mode eigenvector. ϕ is an arbitrary phase factor and is set to zero by default. (A non-zero ϕ would shift the displacements by part of a wave period, and provided the chosen supercell expansion is commensurate with the wavevector $\mathbf{q}$ this should not change the energy.)

In our work, the mode following was performed using the `ModeMap` code,[18] which can be used to prepare sequences of structures diplaced along the modes and to characterise and analyse the resulting mode PES. The code uses `Phonopy` to create modulated structures with displacements over a range of amplitudes along one or two phonon modes frozen in (i.e. 1D or 2D maps).

In order to locate the global energy minimum on the $Bi_2Sn_2O_7$ PES, we begin with a force-constant calculation on the high-symmetry, high-temperature γ structure using a 2×2×2 supercell expansion of the primitive cell. γ-$Bi_2Sn_2O_7$ has multiple imaginary modes in the phonon dispersion, and we tracked the routes from all these modes until each branch terminated in a dynamically-stable structure with no imaginary modes in the dispersion. This is an entirely first-principles approach that requires only the coordinates of the high-

temperature/high-symmetry phase as input and can identify both the (meta-)stable end points and the intermediate structures connecting them. The workflow of this method is outlined in Figure S1.

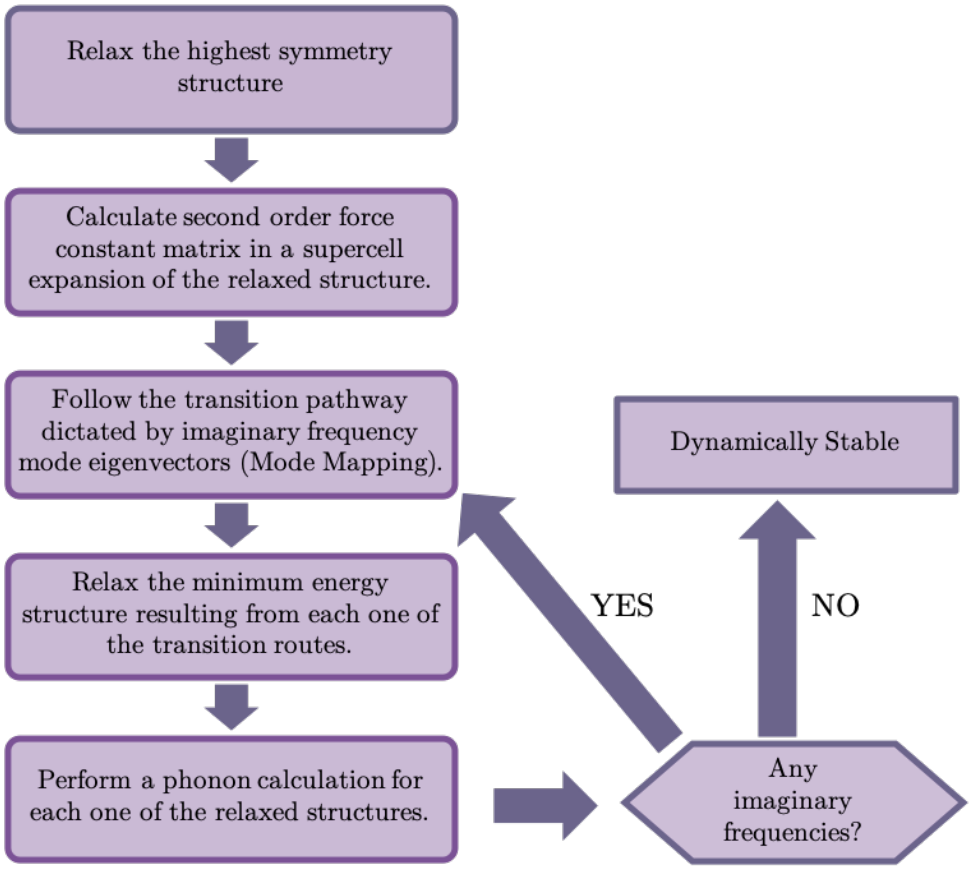

Figure S1: Overview of our *ab intio* lattice dynamics approach to exploring the structural potential-energy surface (PES) of $Bi_2Sn_2O_7$. Starting from the high-symmetry/high-temperature γ phase, which has multiple imaginary modes in the harmonic phonon dispersion, we perform one-dimensional displacements along each independent imaginary mode to locate the energy minimum. The minima along the mode PES curves are optimised and symmetrised, and the phonon dispersion curves of the optimised structures are evaluated to assess the dynamical stability. This process is repeated iteratively until each branch terminates in a dynamically-stable structure with no imaginary modes in the dispersion.

Single-point energy calculations are performed on the distorted structures to generate PES maps showing the change in energy as a function of Q along the imaginary harmonic modes. The PES curves associated with these modes are anharmonic and typically take the form of a double well (DW) potential-energy curve.

The minimum-energy structure from the DW PES is identified and relaxed. This additional relaxation is required for the following two reasons. Firstly, the harmonic approximation only takes into account the local curvature of the PES at the initial geometry, and the minimum of the DW, away from this geometry, may not always correspond to an energy minimum or maximum with net zero forces on the atoms. Where this is the case, the additional relaxation step speeds up locating stationary points on the PES. Secondly, distortions along the harmonic modes do not allow for relaxation of the cell shape and volume, which may further lower the energy.

After relaxation, the structures are symmetrised to a tolerance of 1×10^{-3} Å. This corrects for small numerical inaccuracies in the DFT optimisations and also allows us to reduce the cell size if the structure found by the mode mapping is a supercell or conventional cell of a smaller primitive. Where this is the case, identifying the primitive cell can make the subsequent phonon calculations less computationally demanding. Given our relatively loose symmetry tolerance, a single-point calculation was performed on each symmetrised structure and compared to the relaxed, unsymmetrised structure to confirm that the total energy and pressure were the same to within 0.1 meV per atom and 0.1 kbar, respectively.

Force calculations are then performed on the symmetrised structures to evaluate the harmonic phonon dispersion curves and classify the structures as dynamically stable or unstable (i.e. energy minima or maxima). If the dispersion has imaginary-mode instabilities, the procedure for mapping the imaginary frequency modes is repeated. For structures with multiple instabilities, each independent (non-degenerate) instability is tracked independently. The mode following is repeated iteratively until it terminates at a structure with no instabilities.

The principal advantage of our method is that it is "guided" by the imaginary harmonic modes from the initial structure, *via* continuous distortions, to local energy minima. However, we only consider distortions along single imaginary modes at any given step, whereas coupling between modes may produce combinations of distortions that lead to different minima. A case in point are degenerate imaginary modes, for which any linear combination of

modes is a valid harmonic eigenvector but may not lead directly to the nearest local minimum on the PES. This is partially mitigated in our procedure by the relaxation step after mode following. Also, since we only follow imaginary modes, each mode mapping step can only lead "downhill" in energy, and the method is therefore not guaranteed to explore the full extent of the PES. Despite these downsides, however, the method is an efficient means to explore the PES of complex multernary structures, and successfully identifies the known β and α_{new} polymorphs of $Bi_2Sn_2O_7$ together with several new metastable phases and energetic maxima along the transition pathways connecting them.

Table S1: Lattice parameters, internal energies relative to the α_{new} phase, and dynamical stabilities of the $Bi_2Sn_2O_7$ structures identified using phonon mode mapping to explore the structural potential-energy surface. The cell volumes V are given approximately relative to the parent γ-$Bi_2Sn_2O_7$ structure with $V = V_{cub}$.

Designation	Space group	No. of atoms	No. of unique sites	Volume	Lattice parameters						$E - E(\alpha_{new})$ / meV atom^{-1}	Dynamically stable?
					a/Å	b/Å	c/Å	α/°	β/°	γ/°		
	*Ima*2 (46)	44	9	$0.5V_{cub}$	7.561	10.686	7.559	90	90	90	+1.74	Unstable
	Cc (9)	44	11	$0.5V_{cub}$	10.662	10.698	7.555	90	134.9	90	+1.39	Unstable
α_{new}	*Cc* (9)	88	22	V_{cub}	13.108	7.559	13.115	90	109.6	90	0	Stable
δ	$P2_12_12_1$ (19)	44	11	$0.5V_{cub}$	7.573	7.573	10.666	90	90	90	+0.87	Stable
ϵ	$Pna2_1$ (33)	44	11	$0.5V_{cub}$	7.560	10.694	7.561	90	90	90	+1.45	Stable
	$R\bar{3}c$ (167)	132	7	$1.5V_{cub}$	7.535	7.535	37.046	90	90	120	+4.00	Unstable
	$P\bar{1}$ (2)	88	48	V_{cub}	7.542	13.062	13.094	80.4	73.3	90	+3.64	Unstable
	$P\bar{1}$ (2)	176	92	$2V_{cub}$	13.081	13.091	15.098	106.7	90.04	99.6	+2.52	Unstable
	$P\bar{1}$ (2)	176	92	$2V_{cub}$	7.554	16.887	19.996	89.9	79.1	77.1	+2.25	Unstable
	$P\bar{1}$ (2)	176	92	$2V_{cub}$	7.553	13.096	26.163	99.6	90.1	106.7	+1.86	Unstable
	$P2_1/c$ (14)	88	24	V_{cub}	13.090	7.564	15.128	90	125.3	90	+0.72	Unstable
β	*Aba*2 (41)	176	24	V_{cub}	7.568	21.393	15.120	90	90	90	-0.11	Unstable
ζ	*Cc* (9)	176	44	V_{cub}	15.120	21.396	7.567	90	90.005	90	-0.19	Stable

1D Vs. 2D Mode-Mapping for Doubly-Degenerate Modes

The "mode-mapping" approach assumes that the PES along each phonon mode is independent and that the harmonic eigenvectors are a good approximation to the true anharmonic motion. These assumptions break down in the case of N-fold degenerate modes because linear combinations of the N mode eigenvectors are also valid harmonic eigenvectors (i.e. arbitrary rotations of the basis spanned by the N eigenvectors are possible). The result is that the true minima may not lie along the mode eigenvectors, and locating them in principle requires the full N-dimensional space spanned by the eigenvectors to be mapped out. However, this can be a very computationally-intensive procedure, and in this study we therefore adopted the pragmatic alternative of mapping the individual modes, selecting the lowest-energy structure, and performing a subsequent relaxation. This approach was explicitly verified for several of the structures with doubly-degenerate imaginary modes by comparing the relaxed structure obtained from the 1D mode mapping with that obtained by mapping the 2D PES spanned by both modes (Figure S2).

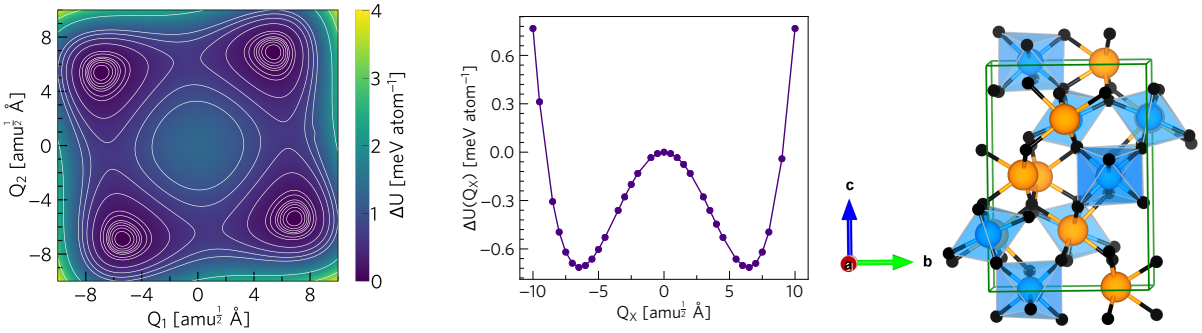

(a) 2D-PES along modes 1 and 2 at X **(b)** DW along mode 1 at X **(c)** $P2_12_12_1$ (19), 44 atoms

Figure S2: (a) Potential-energy surface (PES) along the doubly-degenerate imaginary modes at the X wavevector in the phonon dispersion of γ-$Bi_2Sn_2O_7$. Although the minima on the full 2D PES in (a) do not line up with the Q_1 and Q_2 axes corresponding to the individual mode eigenvectors, an equivalent structure (c) is obtained by relaxing the lowest-energy structure from the 1D slice of the PES shown in (b).

Phonon Dispersion Curves of the *Ima*2 and *Cc* Structures from the Γ-Point Instability in γ-$Bi_2Sn_2O_7$

Starting from the Γ-point instability in γ-$Bi_2Sn_2O_7$, we obtained the α_{new} phase in three mode-mapping steps *via* two intermediate *Ima*2 and *Cc* structures. Figure S3 and Figure S4 show the structures together with the phonon dispersion curves and the double-well potential-energy surfaces along the imaginary modes followed to the next mapping step.

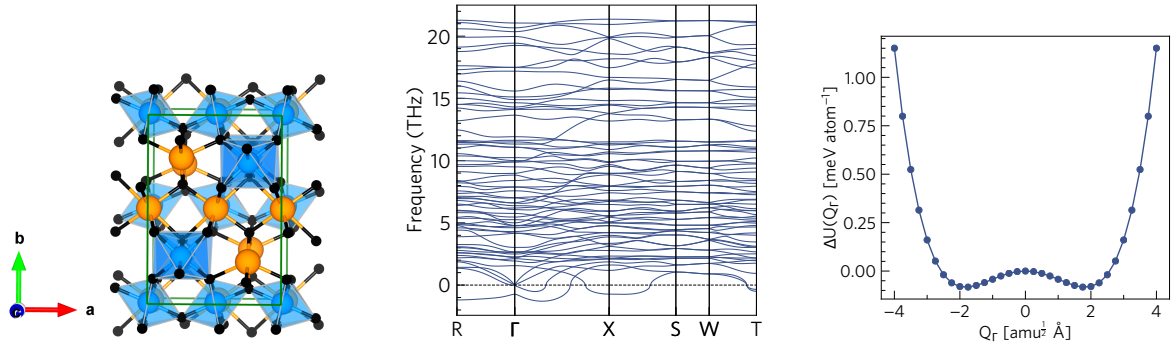

(a) *Ima*2, 44 atoms **(b)** Phonon dispersion of *Ima*2 structure **(c)** DW along mode 1 at Γ

Figure S3: (a) Optimised and symmetrised *Ima*2 structure obtained by mapping the Γ-point imaginary modes in γ-$Bi_2Sn_2O_7$ (Bi - orange, Sn - blue, O/O′ - black). (b) Phonon dispersion. (c) Double-well (DW) PES spanned by the imaginary mode at Γ in (b).

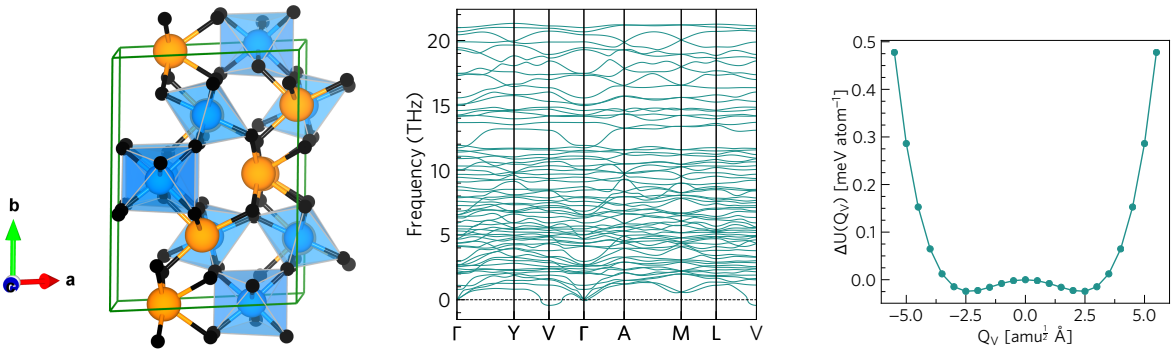

(a) *Cc*, 44 atoms **(b)** Phonon dispersion of *Cc* (44 atoms) structure **(c)** DW along mode 1 at V

Figure S4: (a) Optimised and symmetrised *Cc* structure obtained from the minimum of the double-well potential-energy surface (DW PES) in Figure S3c. (b) Phonon dispersion. (c) DW PES spanned by the imaginary mode at V in (b). The minimum-energy structure on the PES in (c) corresponds to the α_{new}-phase.[13]

Phonon Dispersion Curve of the $P2_12_12_1$ Structure from the X-point Instability in γ-$Bi_2Sn_2O_7$ using Different Supercell Expansions

Mapping the instabilities at X and W in γ-$Bi_2Sn_2O_7$ led to two new metastable structures. As shown in Figure S5, the dispersion of the $P2_12_12_1$ δ-$Bi_2Sn_2O_7$ structure obtained with a $2 \times 2 \times 1$ supercell expansion shows imaginary modes at the $\mathbf{q}_Z = (0, 0, \frac{1}{2})$ wavevector. However, the supercell is not commensurate with this $\mathbf{q}$-point, and thus the frequencies cannot be evaluated exactly and are obtained by Fourier interpolation. When the supercell is increased to a $2 \times 2 \times 2$ expansion, which is commensurate with Z, this imaginary mode disappears, but an acoustic branch along the $\Gamma \rightarrow$ Z path becomes imaginary. Since this is not present using the smaller supercell, we also consider this to be an interpolation artefact. This could in principle be tested by performing calculations with a larger supercell expansion, but the required supercell would contain at least 704 atoms, making the calculation infeasible.

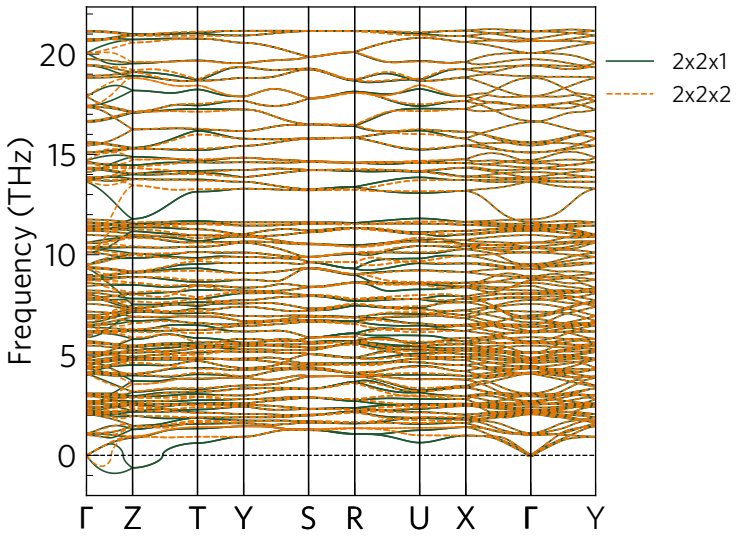

Figure S5: Phonon dispersion curves of the $P2_12_12_1$ structure (denoted δ-$Bi_2Sn_2O_7$ in the text) obtained using $2 \times 2 \times 1$ (solid green) and $2 \times 2 \times 2$ (dashed orange) supercell expansions with 176 and 352 atoms respectively.

Phonon Dispersion Curve of the $R\bar{3}c$ Structure from the L-point Instability in γ-$Bi_2Sn_2O_7$

Starting from the L-point instability in γ-$Bi_2Sn_2O_7$, we again obtain the α_{new} phase, this time in two mode mapping steps *via* an intermediate $R\bar{3}c$ structure shown in Figure S6.

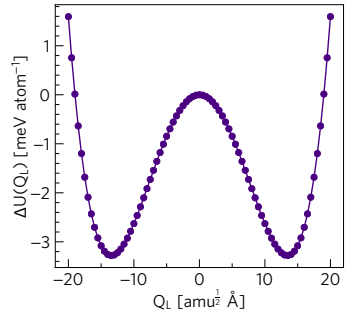

(a) DW along mode 1 at L

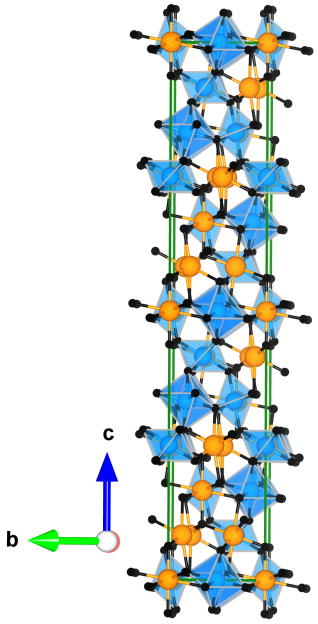

(b) $R\bar{3}c$, 132 atoms

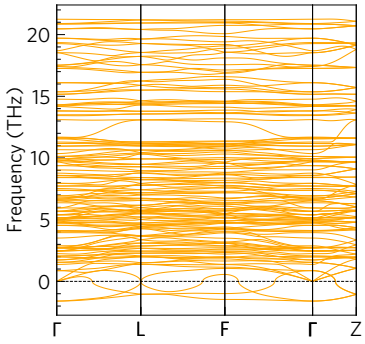

(c) Phonon dispersion of $R\bar{3}c$ structure

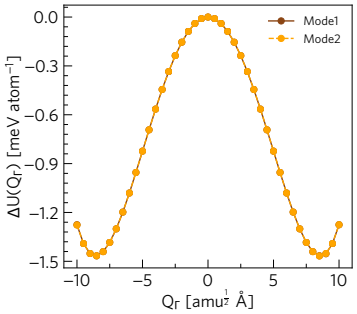

(d) DW along modes 1 and 2 at Γ

Figure S6: (a) Double-well potential-energy surface (DW PES) along the imaginary mode at L in the phonon dispersion curve of γ-$Bi_2Sn_2O_7$. (b) Optimised and symmetrised $R\bar{3}c$ structure obtained as the minimum of the PES in (a). (c) Phonon dispersion of the structure in (b) showing several imaginary modes. (d) DW PES curves spanned by the two imaginary modes at Γ in (c), the minima of which lead to α_{new} after relaxation.

Mapping the Instabilities in the Intermediate Structures

We also mapped the instabilities in the intermediate *Ima*2 and $R\bar{3}c$ structures obtained by mapping the Γ- and L-point instabilities in γ-$Bi_2Sn_2O_7$, respectively.

*Ima*2 Structure

Figure S7 shows the transition pathways from the imaginary modes at X and R in the dispersion of the *Ima*2 structure. The dispersion has imaginary modes at the R, Γ, X and T wavevectors. Following the imaginary mode at X leads to a $Pna2_1$ structure equivalent to that obtained *via* the W-point instability in γ-$Bi_2Sn_2O_7$ (denoted ϵ-$Bi_2Sn_2O_7$ in the text). Following the modes at Γ and R both lead to α_{new}. Following the mode at T does not lower the energy, and the imaginary frequency is therefore an interpolation artefact.

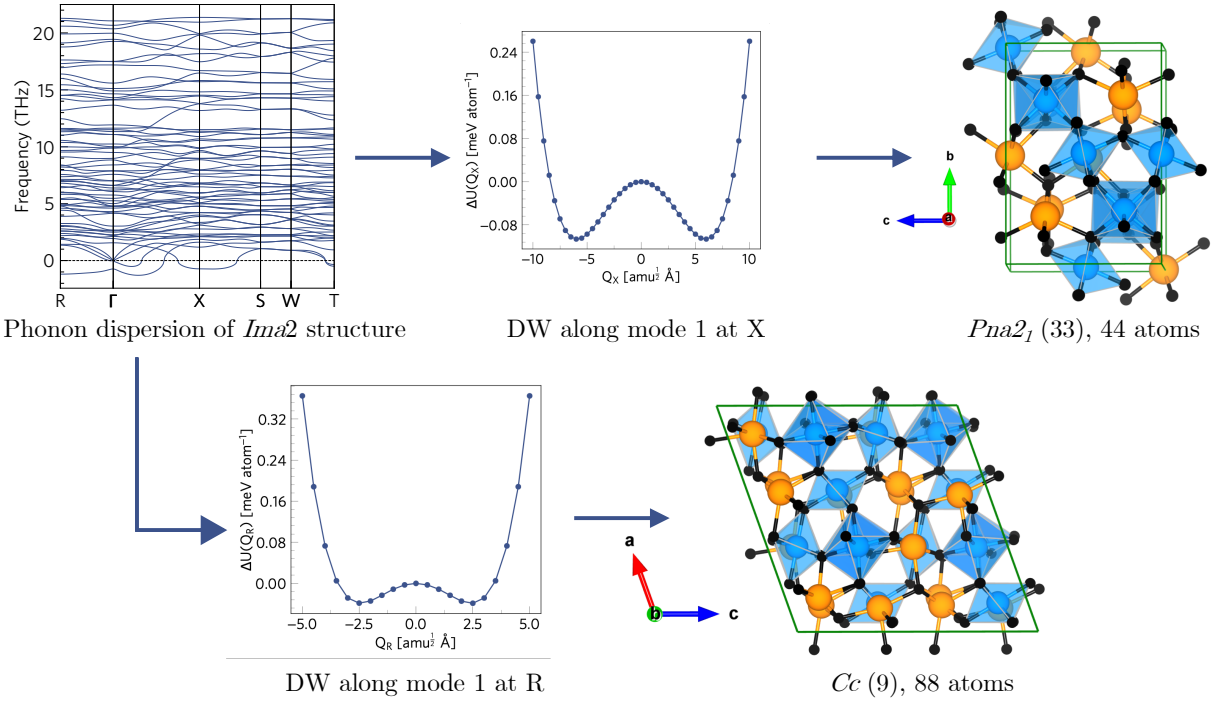

Figure S7: Transition pathways from the imaginary modes at X and R in the phonon dispersion of the intermediate *Ima*2 structure (top left). Following the mode at X leads to ϵ-$Bi_2Sn_2O_7$ ($Pna2_1$; top row). Following the mode at R leads to α_{new} (bottom row).

$R\bar{3}c$ Structure

The $R\bar{3}c$ structure has imaginary modes at all the high-symmetry **q**-points in the Brillouin zone, *viz.* Γ, Z, F and L (Figure S6c).

Mapping the instabilities at Γ and Z lead to the new structural model suggested for the α phase (i.e. α_{new}).[13] Mapping the F-point instability leads to the $P2_1/c$ structure shown in Figure S8b. The phonon dispersion curve of the $P2_1/c$ structure (Figure S8c) has imaginary modes at Γ and Y. Mapping the Y-point mode does not lead to a DW and so the imaginary frequency is an interpolation artefact, while mapping the Γ-point instability (Figure S8d) leads to the structural model of the intermediate-temperature β phase proposed by Lewis *et al.*[13]

Mapping the L-point instability leads to a $P\bar{1}$ structure (Figures S9a and S9b). The phonon dispersion of this structure shows several imaginary modes across the Brillouin zone. Mapping the instability at Γ leads to α_{new}, while the instabilities at Z, V and R lead to the $P2_1/c$ structure shown in Figure S8b, which ultimately leads to the β phase.[13] The other instabilities lead to $P\bar{1}$ structures (Figure S10) – the instabilities at U and X led to the same structure, while the instabilities at Y and T lead to two distinct additional structures. The phonon calculations on these phases were done using a 1×1×1 supercell (i.e. the unit cell), and thus only the Γ-point instabilities are meaningful as other wavevectors are not commensurate with the unit cell. The position of these structures on the tree diagram (Figure 5 in text) suggests they would eventually lead to the α or β phases, which in turn suggests either a large number of stationary points on the structural PES close to these polymorphs, or that there are multiple minima on the PES corresponding to these polymorphs.

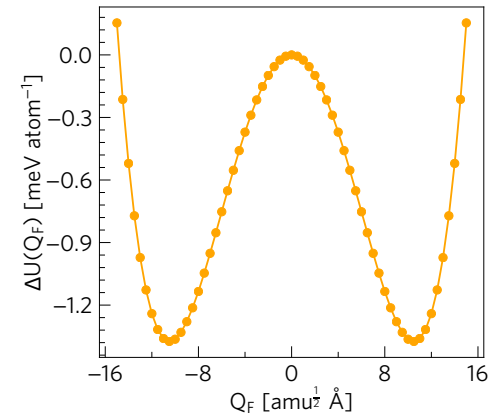

(a) DW along mode 1 at F

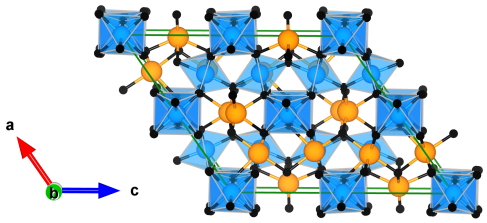

(b) $P2_1/c$, 88 atoms

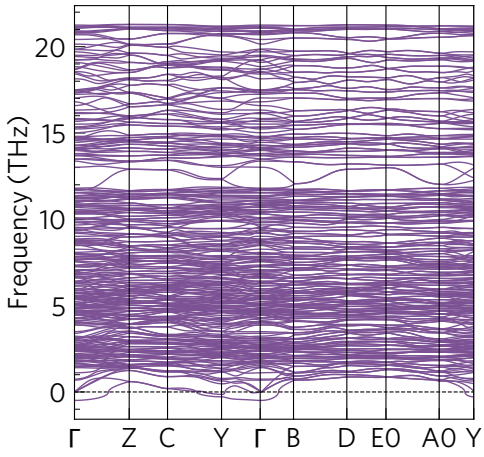

(c) Phonon dispersion of $P2_1/c$ structure

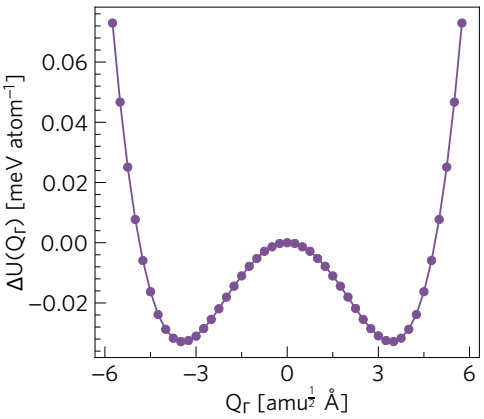

(d) DW along mode 1 at Γ

Figure S8: (a) Double-well potential-energy surface (DW PES) obtained by mapping the first imaginary mode at the F point in the phonon dispersion of the $R\bar{3}c$ structure (Figure S6c). (b) Relaxed and symmetrised $P2_1/c$ structure from the minimum in (a). (c) Phonon dispersion of the structure in (b). (d) DW PES along the Γ-point instability in the $P2_1/c$ dispersion in (c), the minimum of which leads to the β structure identified by Lewis *et al.*[13]

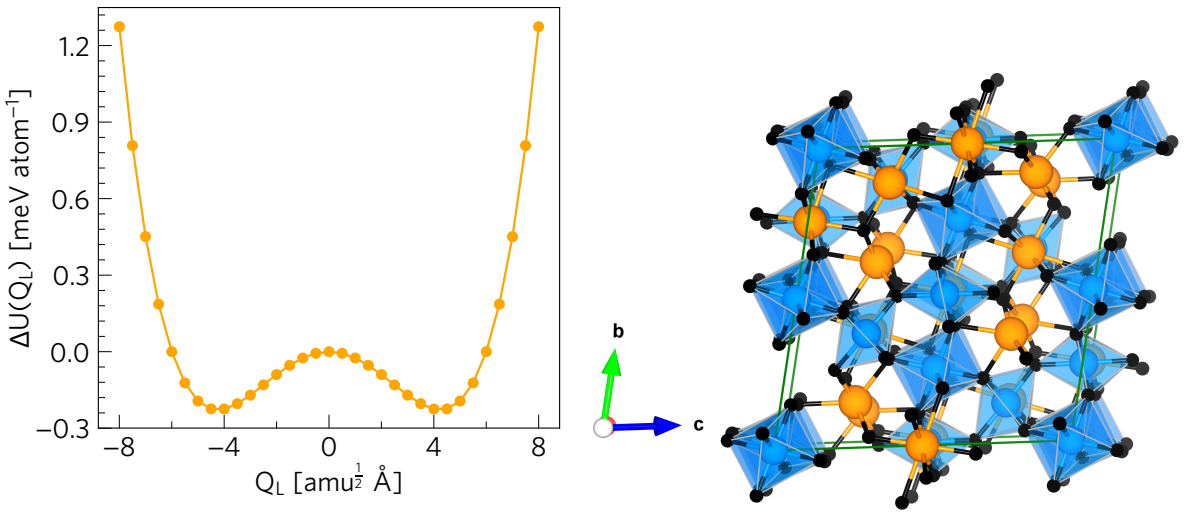

(a) DW along mode 1 at L **(b)** $P\bar{1}$, 88 atoms

Figure S9: (a) Double-well potential-energy surface (DW PES) obtained by mapping the imaginary mode at the L point in the phonon dispersion curve of the $R\bar{3}c$ structure (Figure S6c). (b) Relaxed and symmetrised $P\bar{1}$ structure from the minimum in (a).

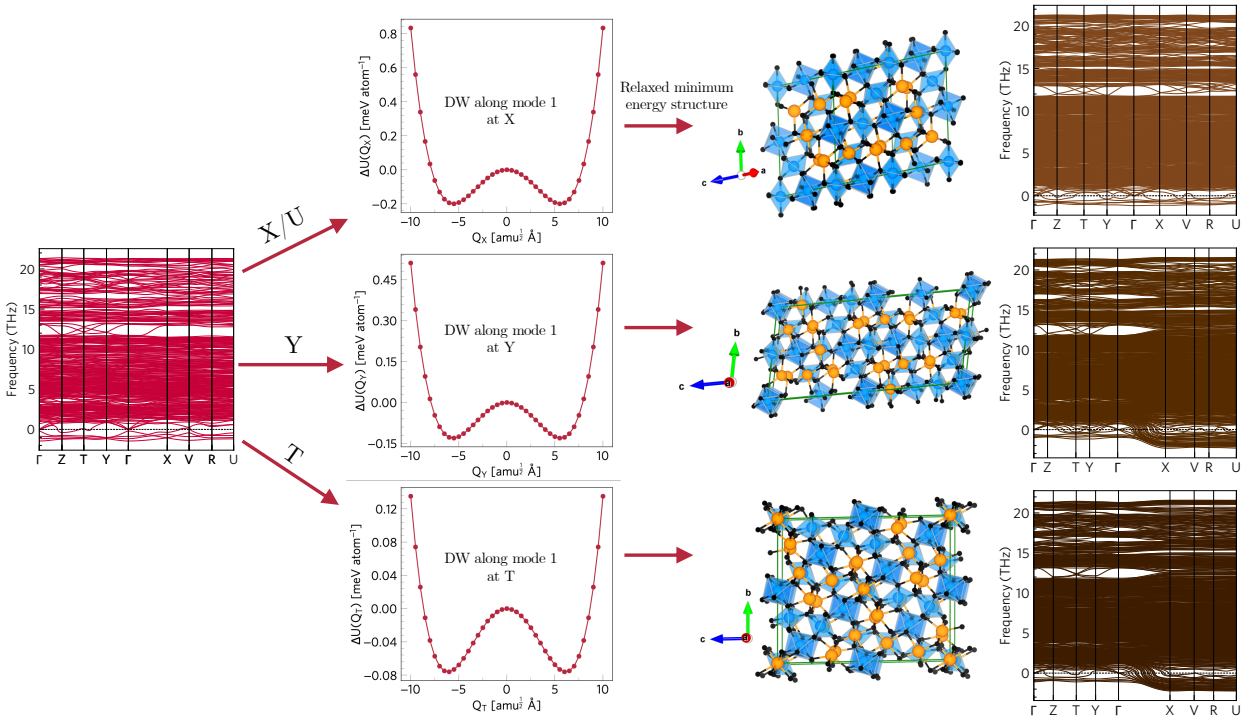

Figure S10: Unique $P\bar{1}$ structures obtained by mapping the instabilities at X, U, Y and T in the phonon dispersion of the $P\bar{1}$ structure (Figure S9b).

Phonon Instabilities in β-$Bi_2Sn_2O_7$

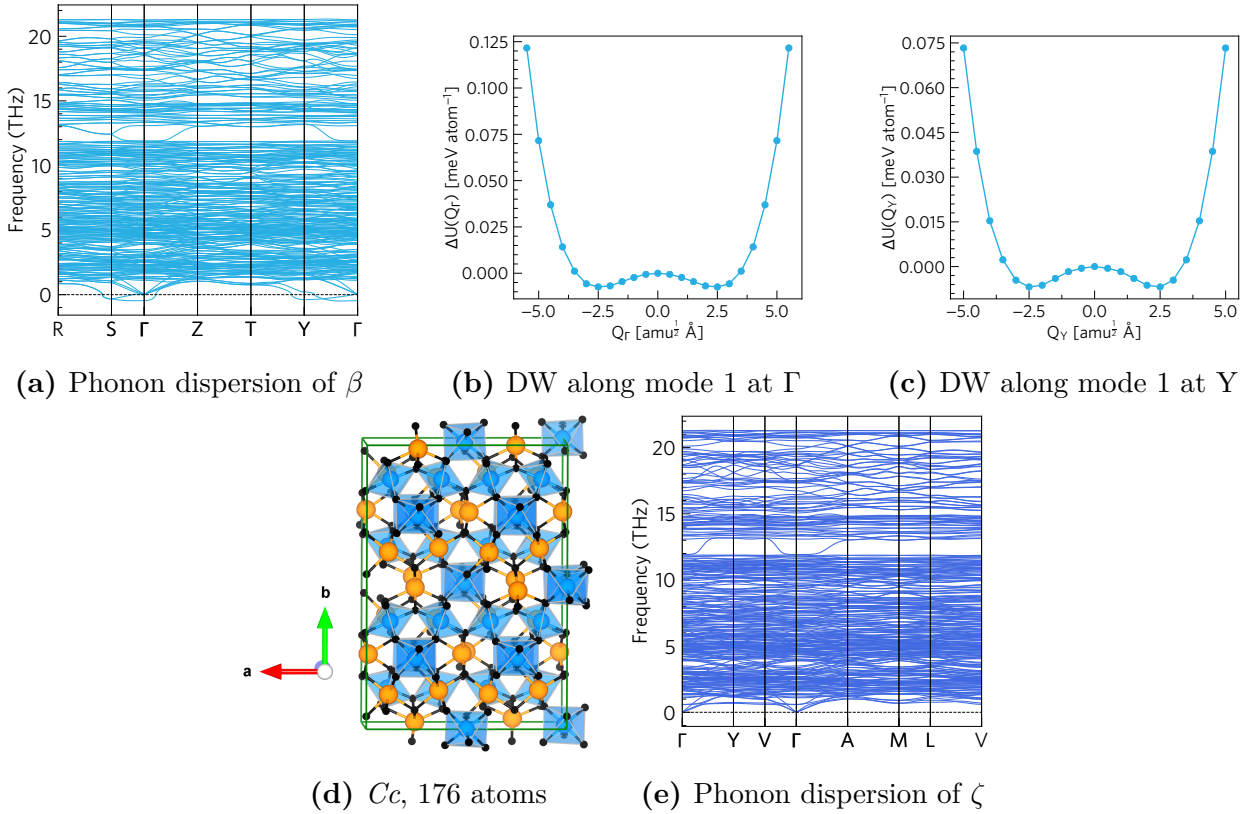

(a) Phonon dispersion of β **(b)** DW along mode 1 at Γ **(c)** DW along mode 1 at Y

(d) *Cc*, 176 atoms **(e)** Phonon dispersion of ζ

Figure S11: The phonon dispersion of the intermediate-temperature β polymorph of $Bi_2Sn_2O_7$ (a) has imaginary modes at Γ, Y and S. The double-well potential-energy surface (DW PES) spanned by the instabilities at Γ and Y (b and c) lead to the optimised/symmetrised *Cc* structure shown in (d), which we denote ζ-$Bi_2Sn_2O_7$, with a very shallow well depth of $\sim 7\times 10^{-3}$ meV per atom relative to the saddle point at $Q = 0$. The phonon dispersion of the ζ structure in (e) shows that this structure is dynamically stable. The instability at S in the β dispersion did not lead to a lower-energy minimum and was therefore identified as an interpolation artefact.

Analysis of the Isotropic Temperature Factors from XRD Measurements

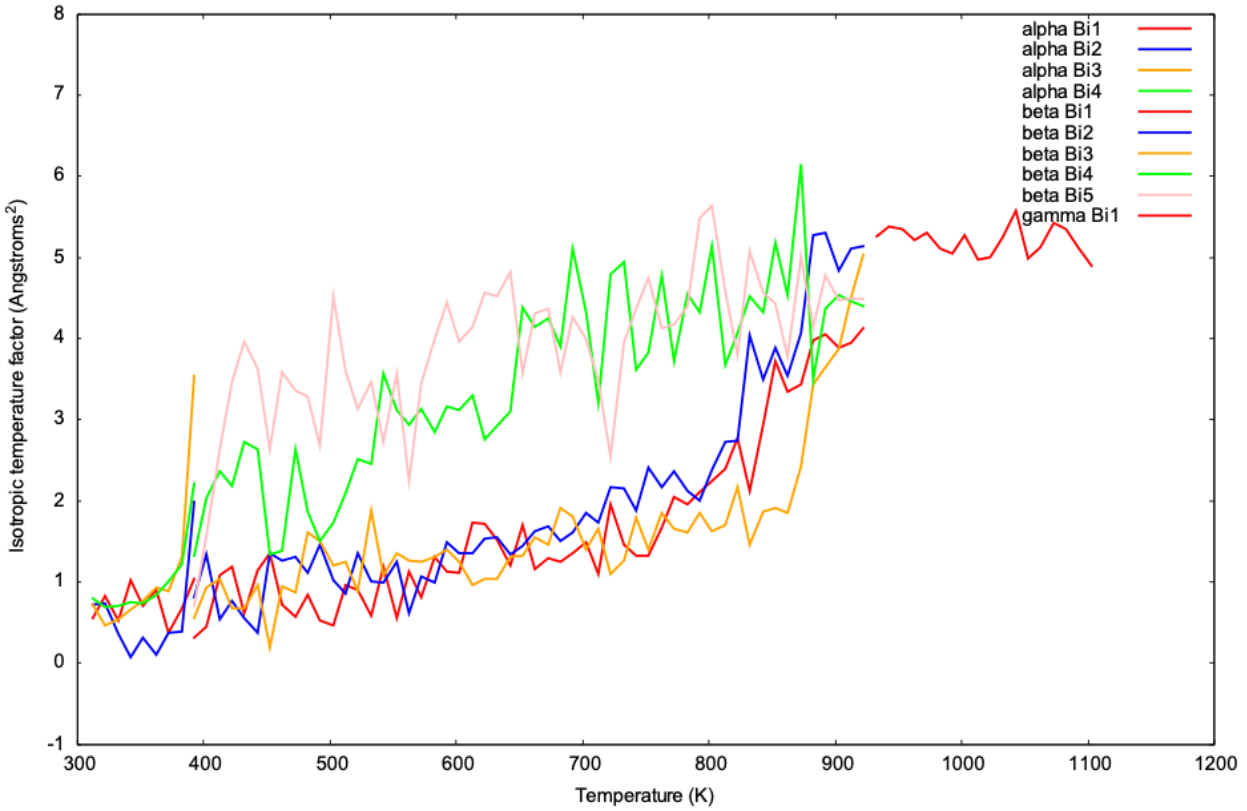

Figure S12: Isotropic temperature factors of the Bi atoms extracted from Rietveld analysis of 81 powder diffraction patterns collected while warming $Bi_2Sn_2O_7$ from 313 to 1103 K (Bruker d8 diffractometer, Anton Paar HTK1200 furnace, Cu Kα radiation, 12-120 degree data collection). In the α phase all 4 Bi sites have similar isotropic temperature factors. In the β phase the temperature factors of Bi4 and Bi5 are significantly higher than Bi1-Bi3 and comparable to those of the single unique Bi in the γ phase. The temperature factors of the Sn sites show a smooth increase with temperature, as do those of the internal Al_2O_3 standard used for temperature and intensity calibration. Both phases are included in the refinements close to the phase transition temperatures. Data values are only plotted where phases are present at >5% weight fraction.

Eigenvectors of the Modes in the γ-to-α Phase Transition

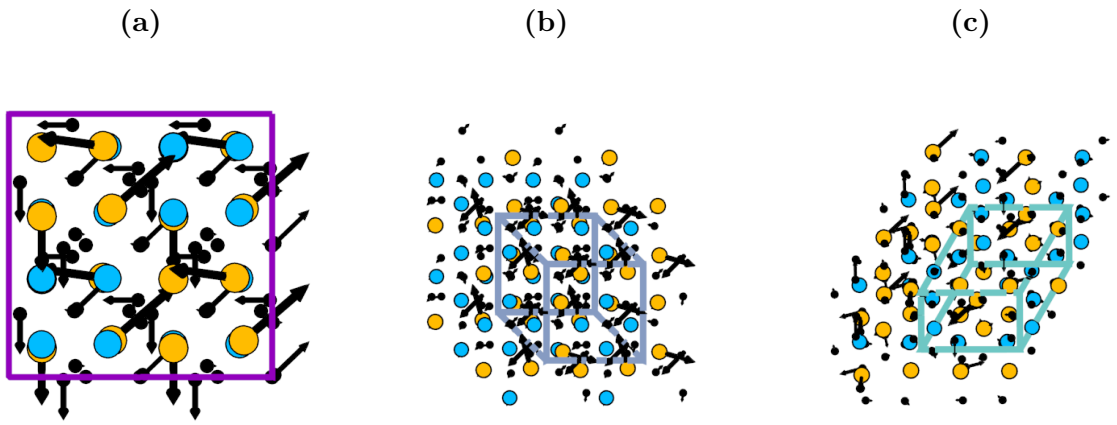

Figure S13: Phonon mode eigenvectors of the imaginary harmonic modes defining one of the transition pathways from the Γ-point instability in γ-$Bi_2Sn_2O_7$ to the α_{new} phase. (a) Atomic displacements associated with one of the Γ-point instabilities in the γ phase, shown in the conventional unit cell. (b) Atomic displacements associated with the Γ-point instability in the *Ima*2 structure, shown in a 2×2×2 supercell. (c) Atomic displacements associated with the V-point instability in the *Cc* structure (44 atoms), shown in a 2×2×2 supercell. In each image the Bi, Sn and O/O′ atoms are shown in orange, blue and black respectively. The eigenvectors indicate coupled rotations of Bi and O atoms, in accordance with previous reports of the transitions between polymorphs being driven by rotations of the Bi_4O' tetrahedra. All three images are shown along the [010] direction and were generated using the `ascii-phonons` software.[19]

References

(1) Kohn, W.; Sham, L. J. Self-Consistent Equations Including Exchange and Correlation Effects. *Phys. Rev.* **1965**, *140*, A1133.

(2) Kresse, G.; Hafner, J. *Ab Initio* Molecular Dynamics for Liquid Metals. *Phys. Rev. B* **1993**, *47*, 558.

(3) Kresse, G.; Hafner, J. *Ab Initio* Molecular-Dynamics Simulation of the Liquid-Metal-Amorphous-Semiconductor Transition in Germanium. *Phys. Rev. B* **1994**, *49*, 14251.

(4) Kresse, G.; Furthmuller, J. Efficiency of *Ab Initio* Total Energy Calculations for Metals and Semiconductors Using a Plane-Wave Basis Set. *Comput. Mater. Sci.* **1996**, *6*, 15.

(5) Kresse, G.; Furthmüller, J. Efficient Iterative Schemes for *Ab Initio* Total-Energy Calculations Using a Plane-Wave Basis Set. *Phys. Rev. B* **1996**, *54*, 11169.

(6) Blöchl, P. E. Projector Augmented-Wave Method. *Phys. Rev. B* **1994**, *50*, 17953.

(7) Kresse, G.; Joubert, D. From Ultrasoft Pseudopotentials to the Projector Augmented-Wave Method. *Phys. Rev. B* **1999**, *59*, 1758.

(8) Perdew, J. P.; Ruzsinszky, A.; Csonka, G. I.; Vydrov, O. A.; Scuseria, G. E.; Constantin, L. A.; Zhou, X.; Burke, K. Generalized Gradient Approximation for Solids and Their Surfaces. *Phys. Rev. Lett.* **2007**, *100*, 136406.

(9) Pulay, P. *Ab Initio* Calculation of Force Constants and Equilibrium Geometries in Polyatomic Molecules. *Mol. Phys.* **1969**, *17*, 197.

(10) Monkhorst, H. J.; Pack, J. D. Special Points for Brillouin-Zone Integrations. *Phys. Rev. B* **1976**, *13*, 5188.

(11) Kahlenberg, V. Structure of γ-$Bi_2Sn_2O_7$ by High Temperature Powder Neutron Diffraction. *Z. Krist. Cryst.* **1997**, *212*, 297.

(12) Evans, I. R.; Howard, J. A. K.; Evans, J. S. O. α-$Bi_2Sn_2O_7$ A 176 Atom Crystal Structure from Powder Diffraction Data. *J. Mater. Chem.* **2003**, *13*, 2098.

(13) Lewis, J. W.; Payne, J. L.; Evans, I. R.; Stokes, H. T.; Campbell, B. J.; Evans, J. S. O. An Exhaustive Symmetry Approach to Structure Determination: Phase Transitions in $Bi_2Sn_2O_7$. *J. Am. Chem. Soc.* **2016**, *138*, 8031.

(14) Parlinski, K.; Li, Z. Q.; Kawazoe, Y. First-Principles Determination of the Soft Mode in Cubic ZrO_2. *Phys. Rev. Lett.* **1997**, *78*, 4063.

(15) Kresse, G.; Furthmüller, J.; Hafner, J. *Ab Initio* Force Constant Approach to Phonon Dispersion Relations of Diamond and Graphite. *Europhys. Lett.* **1995**, *32*, 729.

(16) Togo, A.; Oba, F.; Tanaka, I. First-Principles Calculations of the Ferroelastic Transition Between Rutile-type and $CaCl_2$-type SiO_2 at High Pressures. *Phys. Rev. B* **2008**, *78*, 134106.

(17) Togo, A.; Tanaka, I. First Principles Phonon Calculations in Materials Science. *Scr. Mater.* **2015**, *108*, 1.

(18) Skelton, J. M.; Burton, L. A.; Parker, S. C.; Walsh, A.; Kim, C.-E.; Soon, A.; Buckeridge, J.; Sokol, A. A.; Catlow, C. R. A.; Togo, A.; Tanaka, I. Anharmonicity in the High-Temperature *Cmcm* Phase of SnSe: Soft Modes and Three-Phonon Interactions. *Phys. Rev. Lett.* **2016**, *117*, 075502.

(19) Jackson, A. J. ascii-phonons. `http://https//github.com/ajjackson/ascii-phonons`.